Supplementary Material

S1: Elastase Infusion Surgery

A small animal anesthesia system (SomnoSuite, Kent Scientific) was used to anesthetize all animals using 1-3% isoflurane and 225 mL/min room air, and toe pinch was used to ensure proper anesthetic depth. Mice were placed on a heated surgical stage (SurgiSuite, Kent Scientific), eye lubricant was applied to prevent corneal desiccation, and depilatory cream was used to remove hair from the abdomen. Aseptic technique was then used to clean and sterilize the animal prior to surgery. A mid-line incision was made through skin and muscle layers, and the organs were retracted to expose the inferior vena cava and aorta. We then used a surgical scope (M60, Leica Microsystems, Wetzlar, Germany) to separate the inferior vena cava and aorta, and temporarily ligate branching arteries. Sutures were also placed below the left renal vein and above the aortic trifurcation to create a 3 mm isolated elastase infusion zone. An aortotomy was created by placing a 30 gauge needle and a thinned polyethylene-10 catheter in the aorta, followed by holding the catheter in place using 6-0 silk suture. Porcine pancreatic elastase (PPE) at 2 U/ml was infused for 10 minutes, followed by closing of the aortotomy using 10-0 suture. Finally, we used 4-0 vicryl and 6-0 prolene sutures to close the muscle layer and skin later, respectively. Buprenorphine (0.03 mg/mL) was subcutaneously injected near the incision site at 0.05 mg/kg for pain management.

S2: Ultrasound Imaging

Mice were imaged using a high-resolution small animal ultrasound system (Vevo2100, FUJIFILM VisualSonics) with a 40 MHz central frequency transducer (MS550D). All animals were anesthetized using 2-3% isoflurane and 1.5 L/min medical grade air. To maintain and monitor healthy vital signs the mice were placed on a heated stage, all four paws were taped to gold electrodes to track heart rate and respiration, and a rectal probe was used to monitor body temperature. The orientation of the stage was adjusted to optimize view of the infrarenal aorta and iliac arteries and to minimize artifacts due to abdominal gas and surgical sutures. Hair on the animal was removed using depilatory cream and transmission ultrasound gel was used as an acoustic coupling agent between the ultrasound transducer and the skin (**Suppl. Fig. 2**).

S3: Murine Ultrasound Data Analysis

S3.1: Diameter and Volume Measurements

We quantified aortic diameters from the long-axis B-mode images, and aortic volumes were acquired from the 3D ultrasound data using the VevoLab software (FUJIFILM VisualSonics). For consistency, AAA diameter measurements were taken in the middle of the infrarenal aorta between the left renal vein and aortic trifurcation for all animals and time points (**Figure 2A**). Control contralateral iliac artery diameter measurements were acquired near the aortic trifurcation and in the middle of the iliac artery (**Figure 3A**), while modified iliac artery diameter measurements were taken proximal and distal to the suture placement (**Figure 3B**). Five measurements were taken from each B-mode image to minimize location-dependent error. We obtained volume measurements by segmenting the infrarenal aorta

using 3D short-axis B-mode data from the left renal vein to the aortic trifurcation, as described previously (**Figure 2B**).[1]

S3.2: Mean and Peak Velocities

To measure centerline blood flow velocity, we acquired velocity waveforms by PWD ultrasound. Cine loop acquisitions over 5 seconds were collected in long-axis along the infrarenal aorta and both the left and right iliac arteries. The waveform data were exported as DICOM files for analysis with a custom MATLAB script to obtain measurements of mean and peak blood flow velocity.[2, 3] As part of the MATLAB script, respiration-induced artifacts were removed to eliminate breathing related velocity errors.

S3.3: Circumferential Cyclic Strain Measurements

Circumferential cyclic strain was calculated using M-mode diameter measurements in the middle of the PPE exposed infrarenal aorta, as well as the left and right iliac arteries. Specifically, the anterior and posterior walls of the aorta were first identified using the echogenicity of the flowing blood. We then measured the minimum (end diastole; D_D) and maximum (peak systole; D_S) inner vessel wall diameter (**Figure 2C**). Green-Lagrange circumferential cyclic strain was calculated using:[4, 5]

$$(1) \qquad E_{\theta\theta} = \frac{1}{2}\left[\left(\frac{D_S}{D_D}\right)^2 - 1\right] x \ 100 \ \%$$

S4: Aortic Segmentation and Centerline Path Extraction

We performed 3D segmentation by first creating control-points along the path that was segmented. This path was then smoothed based on control points using Fourier mode

number of 10. Contours were then created along the path to segment both the lumen and the outer wall of the diseased and projected healthy aorta. After segmentation we created a model that allowed us to extract the centerline path of the vessel, which was used to quantify the magnitude and direction of centerline deviation.

S5: Tissue Processing, Histology, and Cell Counting

The infrarenal aorta was resected en bloc with the adjacent vena cava, renal arteries, and kidneys. The bottom half of this tissue segment was carefully dissected to separate the aorta from adjacent tissues, stored in RNA later (Qiagen), and snap-frozen in liquid nitrogen for storage at –80°C. The upper half and adjacent tissues were fixed in 4% paraformaldehyde (Thermo Fisher Scientific) overnight for histology. Five μm sections of paraffin-embedded samples were mounted on SuperFrost © slides (Menzel) and stained with hematoxylin and eosin (H&E) and Elastica van Gieson (EvG). Finally, ImageJ was used to determine the cellular content in H&E aneurysm sections by counting cell nuclei in a 1 cm^2 region of interest (including the aortic media and intima) three times at 100x magnification.[6, 7]

S6: Gene Expression Experiments

Gene expression was analyzed with quantitative RT-PCR. Total cellular RNA was extracted from 5 control aortae (non-operated C57BL/6J wild-type mice, 12 weeks old) and all PPE-treated mice in the study with TRIzol reagent (Invitrogen Life Technologies) as recommended by the manufacturer. RNA integrity was verified using the Experion automated electrophoresis station (Bio-Rad Laboratories Inc). Primer sets (Qiagen) were designed using PrimerBlast (http://www.ncbi.nlm.nih.gov/tools/primer-blast/) for IL-6

(Mm00446190_m1), VEGFA (Mm00437306_m1), KLF4 (Mm00516104_m1), and TGFß (Mm01178820_m1). The housekeeping gene was β-actin (ACTB) (Mm00607939_s1). For first-strand cDNA synthesis, 1 μg of total RNA was employed using the iScriptcDNA synthesis kit (Bio-Rad). Quantitative PCR was performed with the qPCRMasterMix kit for SYBR Green (BioRad). All PCR were carried out with a CFX96 RT-PCR system (Bio-Rad) operated by CFX Manager software (version 3.0). Each run was 40 cycles with denaturing conditions at 95°C for 15 s, annealing at 60°C for 1 min and extension at 65°C for 3 minutes. Results are displayed using the $2^{-\Delta\Delta Ct}$ value for fold change of expression compared to non-PPE-treated control aortae.

S7: Ki67 and TGFβ Immunohistochemistry

Cryosections were for thawed for 20 minutes and fixed for 20 minutes in 4% PFA. To quench endogenous peroxidase activity, slides were incubated for 30 minutes in 3% H2O2 (Merck) at room temperature. Immunohistochemistry protocol for Ki67 and TGFβ was executed by first blocking for 1 hour in 5% normal goat serum with 1% bovine serum albumin (Sigma), followed by overnight incubation at 4°C with primary antibody diluted in blocking serum (Ki67 1: 200, Abcam; TGF-b-1 1:100, ab92486 rabbit polyclonal Abcam). The sections were then diluted for 30 minutes with biotinylated secondary antibody (goatantirabbit,1:200inPBS-T 5% goat serum). Afterwards the Vectastain ABC Reagent was applied according to the manufacturer's protocol (Vector Laboratories). Nuclear counterstaining was performed with DAPI (diluted 1:2000 in water; Carl Roth) or Mayer's hematoxylin (Carl Roth) for 20 minutes at room temperature. Negative control experiments, including incubation with phosphate buffered saline instead of primary antibody, were done for each antibody. Slides were then photographed with a Keyence BZ9000 microscope

(Keyence, Kyoto, Japan) or scanned with a NanoZoomer 2.0-HT Digital slide scanner C9600 (Meyer Instruments, Hamamatsu, Japan) and images were taken with the NDP.view2 software (Meyer Instruments, Hamamatsu, Japan).

Case Report 1: AAA with Left Common Iliac Artery Occlusion

Tissue was acquired from a 77 year old female patient with an asymptomatic fusiform AAA of 58 mm at the time of operation. The aneurysm had been under surveillance for 9 years from a diameter of 44mm, suggesting a rather slow growth. Additionally, the patient had a complete occlusion of the left common iliac artery, without signs of claudication or leg ischemia on the left side, due to good collateralization. She was operated with an aorto-biiliac graft interposition with a transperitoneal open approach. The patient also had chronic kidney disease (KDIGO III) and smoked until the time of surgery, as well as other co-morbidities including hyperlipidemia and hypertensive disease.

Case Report 2: AAA with Right Leg Amputation

Tissue was acquired from a 67 year old female with asymptomatic AAA of 51 mm. The patient was under surveillance for 7 years until reaching a surgical threshold. She had undergone above the knee right leg amputation 7 years prior due to leg ischemia as a result of a thrombosed popliteal aneurysm (PAA). The left leg had been treated with a femoropopliteal bypass due to PAA of 27 mm 6.5 years prior. She had a pronounced cardiovascular risk profile with metabolic syndrome, including hypertension, hyperlipidemia, type II diabetes and obesity, as well as other co-morbidities such as heart insufficiency NYHA II and chronic obstructive pulmonary disease. Additionally she had been a longtime smoker before the major amputation. The patient was operated with a tube graft interposition by an open retroperitoneal approach. Although surgery went well and without complications, the

patient never recovered from anesthesia due to a cerebral non-perfusion caused by subarachnoidal hemorrhages due to hypertensive emergency during anesthesia induction.

S8: Statistical Methods

We used two-way analysis of variance (ANOVA) with Tukey's HSD post-hoc analysis to determine statistical significance for aortic diameter, volume/length, and strain data, as well as both aortic and iliac artery mean and peak velocities. Additionally, we used one-way ANOVA with Tukey's HSD post-hoc analysis to determine statistical significance for day 56 iliac artery strain, mean velocity, diameter. Further, one-way ANOVA with Tukey's HSD post-hoc was also used to evaluate significance for aortic ΔCt gene expression, cell counting, and centerline deviation magnitude data. Centerline deviation direction statistics was performed using MATLAB CircStat Toolbox.[8] All values are reported and plotted as average ± standard deviation.

References

1 Phillips EH, Yrineo AA, Schroeder HD, Wilson KE, Cheng J-X, Goergen CJ: Morphological and biomechanical differences in the elastase and AngII apoE−/− rodent models of abdominal aortic aneurysms. BioMed research international 2015;2015

2 Cuomo F, Ferruzzi J, Humphrey JD, Figueroa CA: An experimental–computational study of catheter induced alterations in pulse wave velocity in anesthetized mice. Annals of biomedical engineering 2015;43:1555-1570.

3 Gaddum NR, Alastruey J, Beerbaum P, Chowienczyk P, Schaeffter T: A technical assessment of pulse wave velocity algorithms applied to non-invasive arterial waveforms. Annals of biomedical engineering 2013;41:2617-2629.

4 Goergen CJ, Barr KN, Huynh DT, Eastham‐Anderson JR, Choi G, Hedehus M, Dalman RL, Connolly AJ, Taylor CA, Tsao PS: In vivo quantification of murine aortic cyclic strain, motion, and curvature: implications for abdominal aortic aneurysm growth. Journal of Magnetic Resonance Imaging 2010;32:847-858.

5 Humphrey JD, DeLange S: An introduction to biomechanics: solids and fluids, analysis and design, ed 2. Springer-Verlag New York, 2015.

6 Schneider CA, Rasband WS, Eliceiri KW: NIH Image to ImageJ: 25 years of image analysis. Nature methods 2012;9:671.

7 Abràmoff MD, Magalhães PJ, Ram SJ: Image processing with ImageJ. Biophotonics international 2004;11:36-42.

8 Berens P: CircStat: a MATLAB toolbox for circular statistics. J Stat Softw 2009;31:1-21.

A: IVC, A, Cr, R, L, Ca
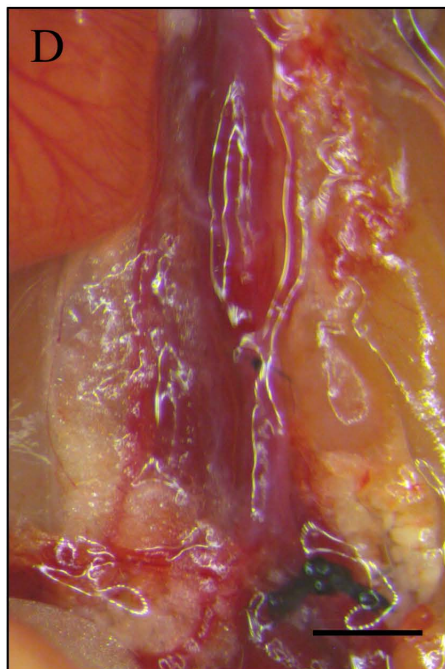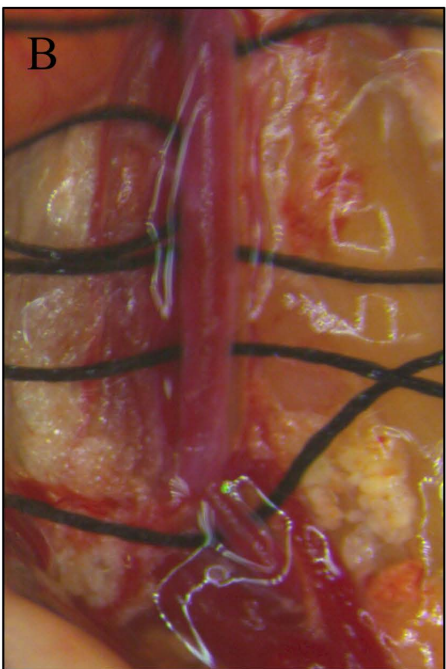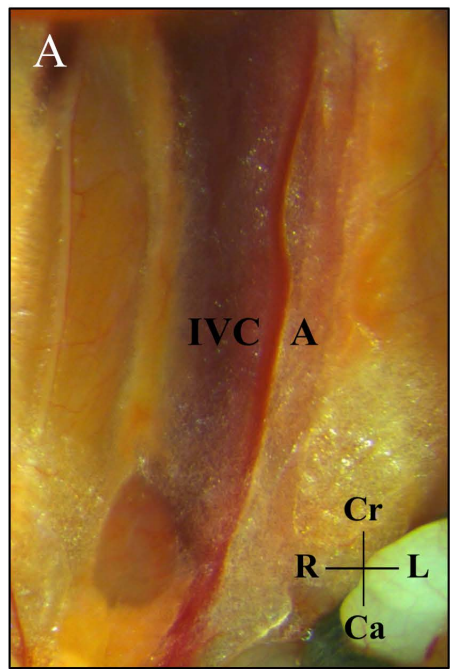
Suppl. Fig. 1: Summary of PPE infusion procedure. Aorta and inferior vena cava were first exposed (A) and separated. 6-0 silk sutures were then placed to temporarily ligate branching vessels and infusion inlet and outlet zones, and permanently placed to partially ligate the iliac artery (B). Catheter was placed in the aorta via aortotomy (C) for 10-minute elastase infusion. Aortotomy was then closed using 10-0 suture, temporary sutures are removed, and single iliac artery was partially ligated (D). Cr: Cranial, Ca: Caudal, L: Left, R: Right. Scale bar denotes 2mm.

2-3% Isoflurane

ECG Electrodes

C57BL/6 Mouse

Heated Stage

Ultrasound Gel

Temperature Probe

40 MHz Transducer

Vevo 2100 Ultrasound

B-Mode

M-Mode

Pulsed Wave Doppler
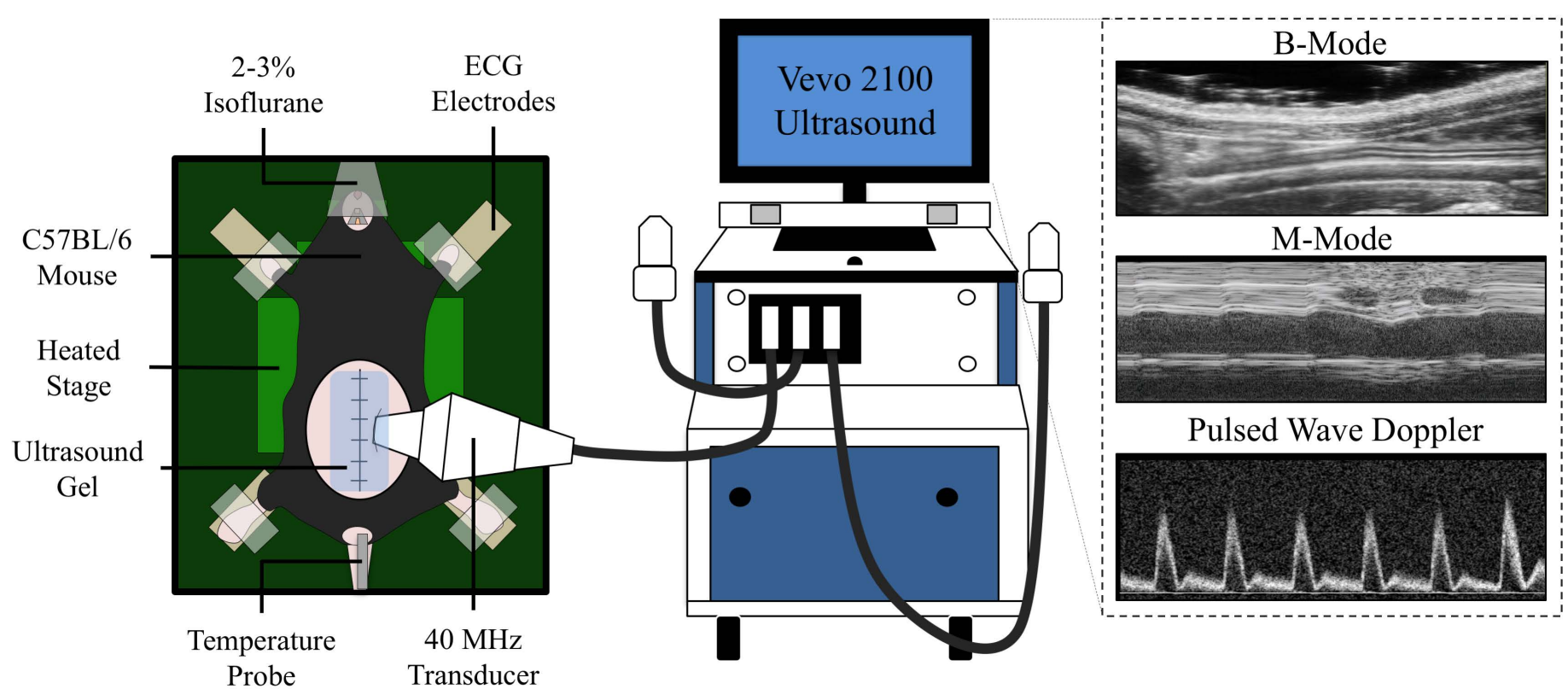
Suppl. Fig. 2: Overview of ultrasound imaging procedure. Mice were anesthetized and placed on a heated stage where heart rate, respiration, and temperature are closely monitored to ensure animal safety. Ultrasound probe was appropriately placed on the animal to minimize artifacts due to suture and intestinal gas. After ensuring proper anesthesia induction, ultrasound imaging was performed to obtain structural and hemodynamic information.
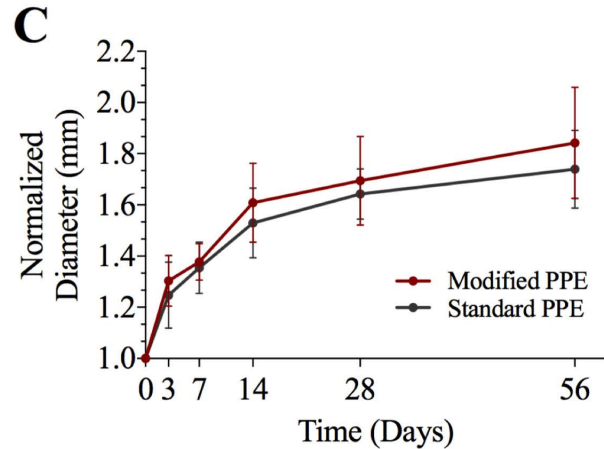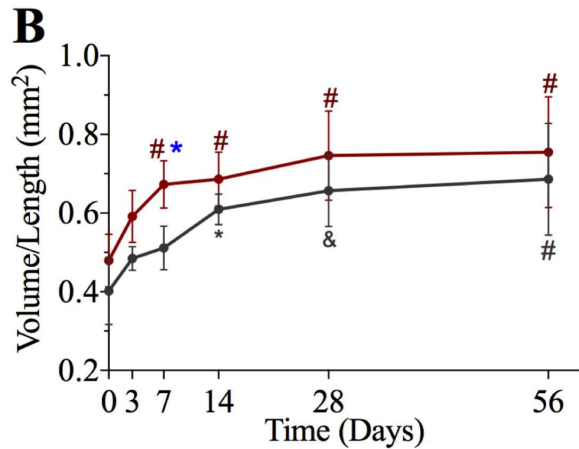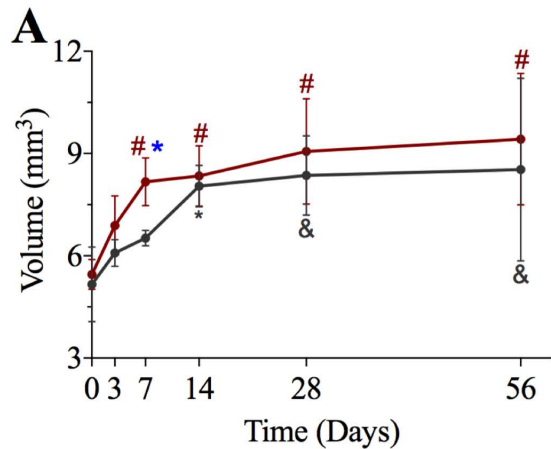
Suppl. Fig. 3: Comparison of aortic volume (A), volume/length (B), and normalized diameter (C) changes over 56 days between the standard and modified PPE groups. Both volume and volume/length reveal rapid aneurysm growth over the first seven days post-PPE infusion. Normalized aortic diameter shows continued AAA growth up to day 56. Statistical significance compared with day 0 and defined at $p<0.05$ (*), $p<0.01$ (&), and $p<0.001$ (#). Blue asterisk represents statistical significance between the standard and modified PPE groups at day 7.
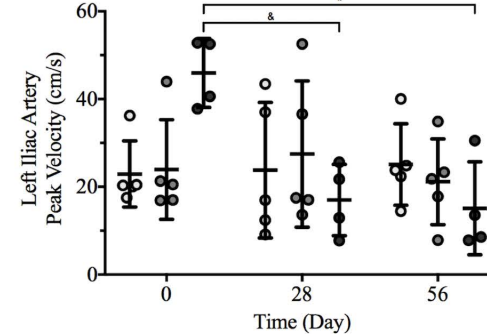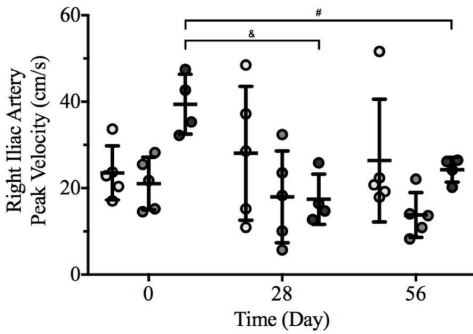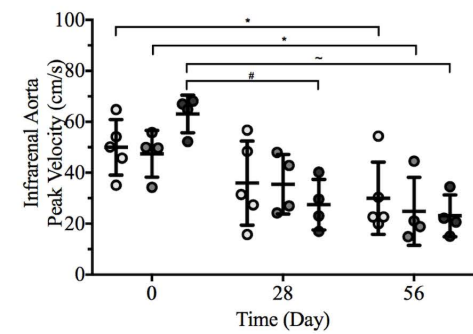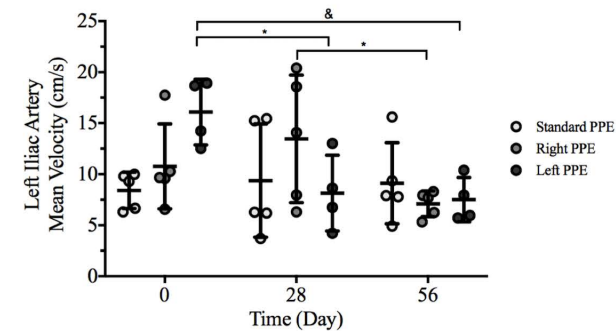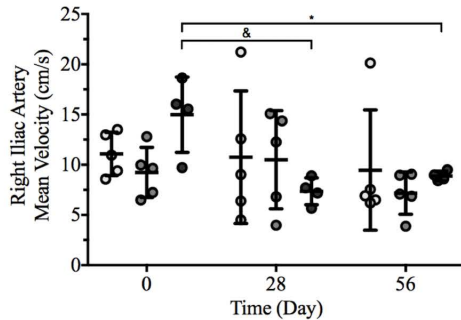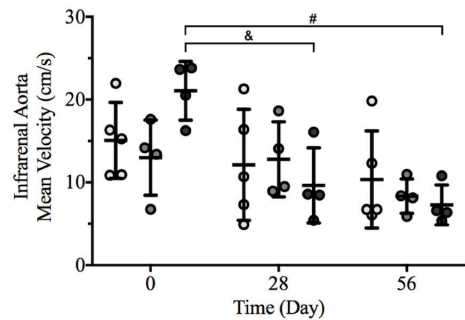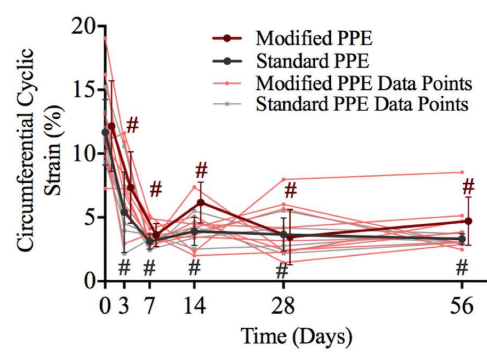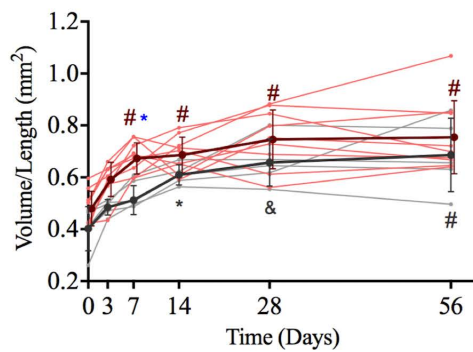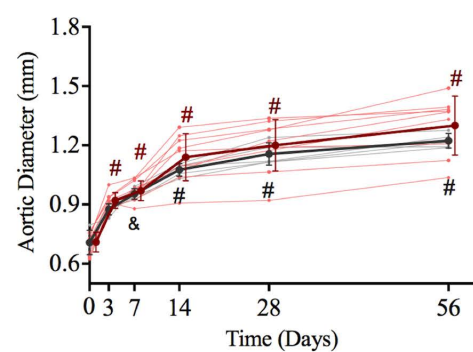
Suppl. Fig. 4: Morphological, kinematic, and hemodynamic changes in infrarenal aorta, and left and right iliac arteries due to PPE infusion and partial iliac ligation. Diameter measurements show gradual increase in AAA size up to day 56, with volume/length showing rapid aneurysm expansion in the first seven days. Circumferential cyclic strain measurements reveal rapid decrease in aortic pulsatility post-PPE infusion for all animals. Mean and peak velocity measurements were averaged over 20 or more cardiac cycles. Infrarenal aorta measurements were acquired in the middle of the aorta, between the left renal vein and aortic trifurcation, and iliac artery measurements were taken distal to suture placement. Overall, infrarenal aorta, and modified left and right PPE velocities decrease after surgical AAA induction and partial iliac ligation, respectively by day 56. Statistical significance defined at $p<0.05$ (*), $p<0.01$ (&), and $p<0.001$ (#).
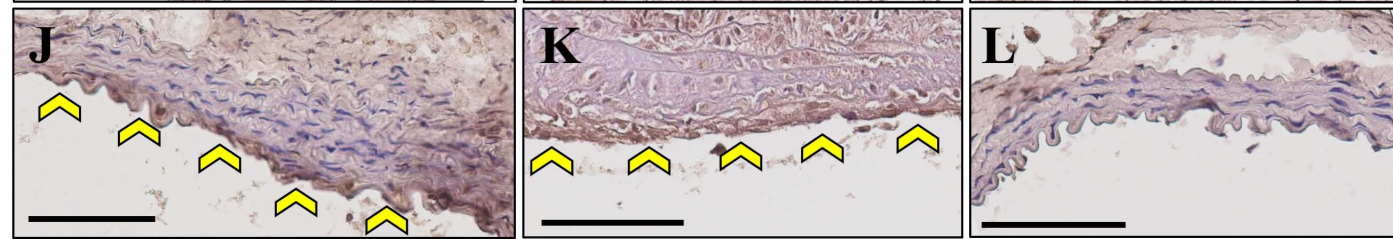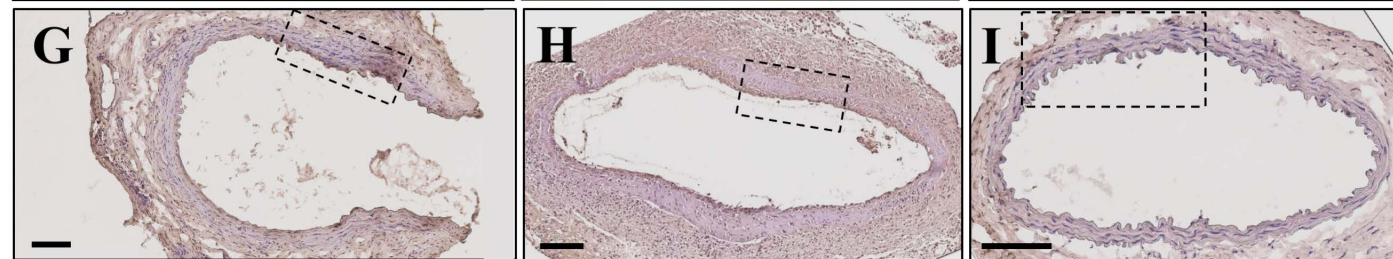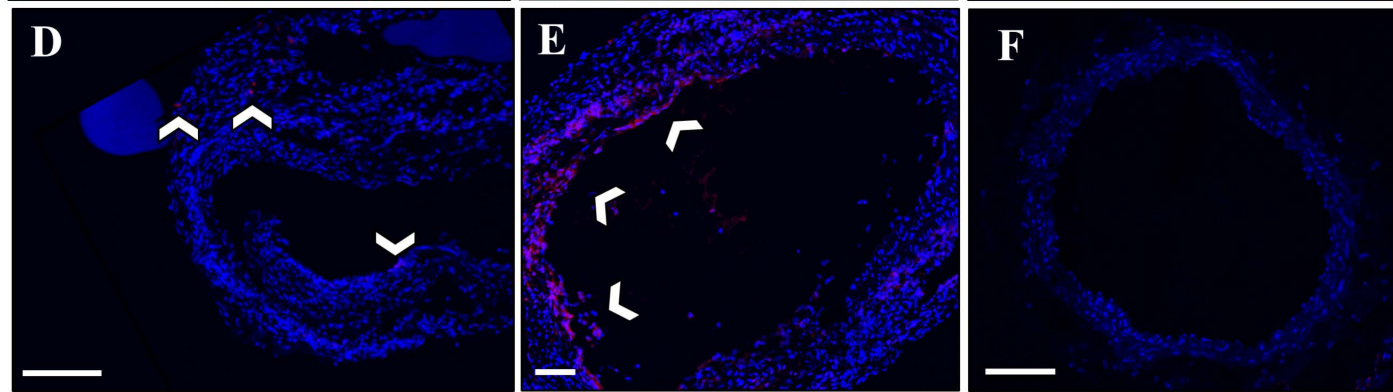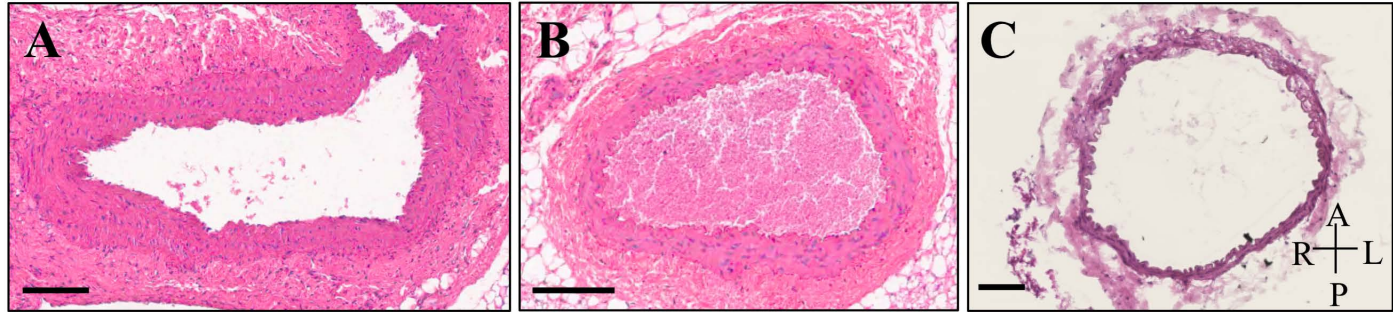
Suppl. Fig. 5: Histological and immunohistochemistry analysis of PPE infused aortic tissue. H&E stained standard (A) and modified (B) PPE aortae showed vessel wall thickening compared to control aortae (C). Ki67 staining confirmed cell proliferation (white arrow) in standard (D) and modified (E) aortae compared to control aortae (F). Immunohistochemistry revealed TGFβ1 expression (yellow arrows) in standard (G,J) and modified (H,K) animals compared to control animals (I,L). A: Anterior, P: Posterior, L: Left, R: Right. Scale bar denotes 100 μm.

Computed Tomography	H&E	EvG	CD34	CD45

A B C D E

F G H I J

Cr
R — L
Ca

Ad
Lu
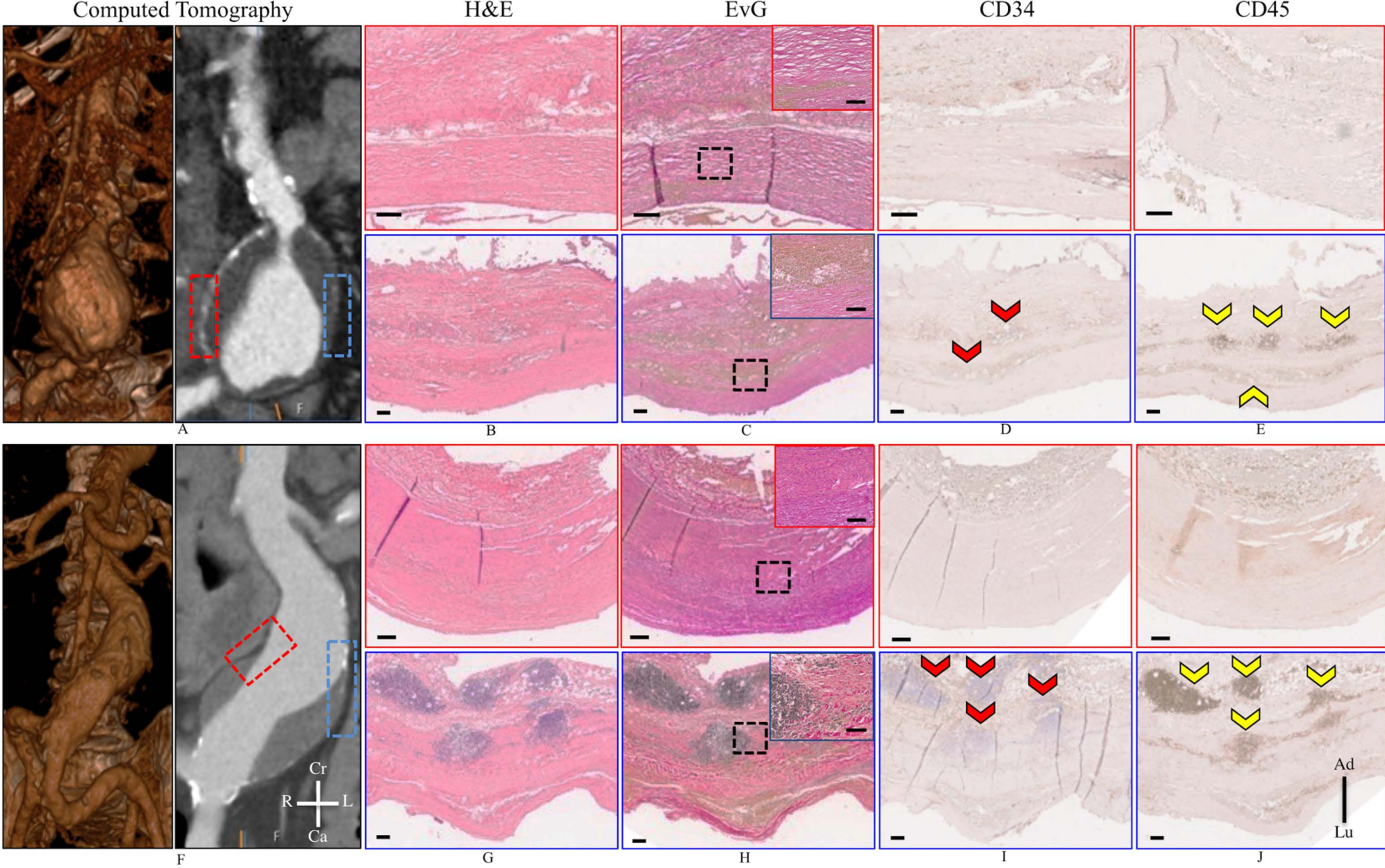
Suppl. Fig. 6: Computed tomography imaging of two AAA patients, one with a left common iliac occlusion (A) and one with a right leg amputation (F), reveals asymmetrical aneurysm formation. Closer examination with H&E staining shows signs of increased cellular infiltration on the left side of the AAA in both the modified left (B) and right (G) iliac outflow. EvG staining reveals widespread destruction of elastin laminar units (C,H). High resolution images of elastin destruction are shown in the EvG insets with the location of the inset shown in black dotted boxes. Cellular infiltrate was primarily comprised of inflammatory cells via CD34 (red arrows; D, I) and CD45 (yellow arrows; E, J) immunohistochemistry. Cr: Cranial, Ca: Caudal, L: Left, R: Right, Av: adventitia, Lu: Lumen. Scale bar denotes 200 μm.

Iliac Artery	Standard PPE		Modifed PPE		Contralateral Control	
	Left Iliac	Right Iliac	Left Iliac	Right Iliac	Left Iliac	Right Iliac
Mean Velocity (cm/s)	9.11 ± 3.97 cm/s	9.46 ± 5.99 cm/s	7.17 ± 2.10 cm/s	7.10 ± 1.26 cm/s	7.51 ± 2.17 cm/s	8.88 ± 0.48 cm/s

Table I: Summary of iliac artery mean velocities for the standard PPE, as well as modified left and right PPE groups at day 56. Standard PPE group shows slightly greater and more variable mean velocities in the left and right iliac arteries.

Day	Measurement	Standard PPE	Left PPE	Right PPE
28	Magnitude	0.02 ± 0.12 mm	0.11 ± 0.06 mm	0.08 ± 0.22 mm
	Direction	170.2 ± 22.5º	189.2 ± 72.6º	66.7 ± 24.3º
56	Magnitude	0.04 ± 0.10 mm	0.12 ± 0.25 mm	0.12 ± 0.10 mm
	Direction	354.2 ± 51.7º	210.0 ± 30.5º	171.3 ± 27.2º

Table II: Day 28 and 56 centerline deviation results showing magnitude and direction of AAA growth in standard PPE, as well as left and right modified PPE groups.